IEEE Photonics Journal
An IEEE Photonics Society Publication

Open Access

Multiple Fano Resonances Control in MIM Side-Coupled Cavities Systems

Volume 7, Number 3, June 2015

Zhao Chen
Xiaokang Song
Gaoyan Duan
Lulu Wang
Li Yu

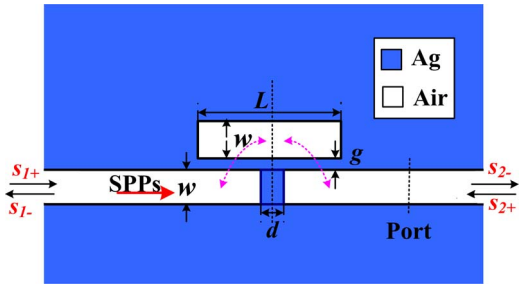

DOI: 10.1109/JPHOT.2015.2433012
1943-0655 © 2015 IEEE

IEEE photonics SOCIETY
IEEE

Multiple Fano Resonances Control in MIM Side-Coupled Cavities Systems

Zhao Chen, Xiaokang Song, Gaoyan Duan, Lulu Wang, and Li Yu

State Key Laboratory of Information Photonics and Optical Communications, Beijing University of Posts and Telecommunications, Beijing 100876, China
School of Science, Beijing University of Posts and Telecommunications, Beijing 100876, China

DOI: 10.1109/JPHOT.2015.2433012
1943-0655 © 2015 IEEE. Translations and content mining are permitted for academic research only. Personal use is also permitted, but republication/redistribution requires IEEE permission. See http://www.ieee.org/publications_standards/publications/rights/index.html for more information.

Manuscript received April 14, 2015; revised May 11, 2015; accepted May 11, 2015. Date of publication May 13, 2015; date of current version June 9, 2015. This work was supported by the National Natural Science Foundation of China under Grant 11374041, Grant 11404030, and by the Fund of the State Key Laboratory of Information Photonics and Optical Communications (Beijing University of Posts and Telecommunications), China. Corresponding author: L. Yu (e-mail: bupt.yuli@gmail.com).

Abstract: We theoretically demonstrate a plasmonic waveguide that allows easy control of the fano profile. The proposed structure is analyzed by the coupled-mode theory and demonstrated by the finite-element method. Due to the interaction of the local discrete state and the continuous spectrum caused by the side-coupled cavity and the baffle, respectively, the transmission spectrum exhibits a sharp and asymmetric profile. The profile can be easily tuned by changing the parameters of the structure. Moreover, the compact structure can easily be extended to several complex structures to achieve multiple fano resonances. These characteristics offer flexibility in the design of the device. This nanosensor yields a sensitivity of ∼1280 nm/RIU and switches with an on/off contrast ratio of about 30 dB. Our structures may have potential applications for nanoscale optical switching, nanosensors, and slow-light devices in highly integrated circuits.

Index Terms: Surface plasmons, fano resonance, resonator, sensor.

1. Introduction

Surface plasmon polaritons (SPPs) are considered to be the most promising candidates for the realization of highly integrated optical circuits, due to their capability to overcome the diffraction limit of light [1]. In particular, the metal-insulator-metal (MIM) waveguides based on SPPs has deep subwavelength field confinements and low bend loss, and thus, it has important applications in highly integrated photonic circuits [2]–[4]. A large number of devices based on MIM waveguides are designed to achieve various functions, such as filters [5]–[8], splitters [9], [10], sensors [11], [12], and demultiplexers [13]–[16]. As a fundamental resonant effect, the Fano resonance, appears as an interference effect between a localized state and a continuum band in quantum or classical systems [17], [18]. Different from the Lorentzian resonance, the Fano resonance exhibits a typical sharp and asymmetric line profile [18], and this specific feature of the Fano resonance promises applications in sensors [12], [19], switches [20], [21], wavelength demultiplexing [22], [23], and so on. Fano resonances have been widely studied in numerous physics systems, such as rings [24], [25], photonic crystal [26]–[28], planar oligomers [29]–[31] and MIM waveguides [12], [22], [32], [33]. Due to the advantage for enhanced bio-chemical sensing, spectroscopy, and multicolor nonlinear processes, the multiple Fano resonances become more important and have gained much

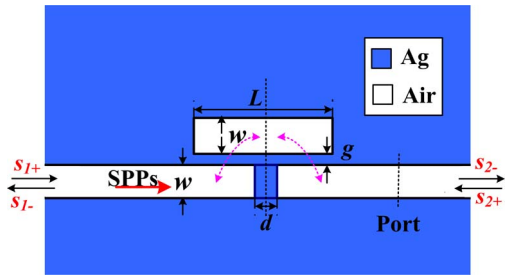

Fig. 1. Schematic of the optical system consisting of a MIM waveguide with a side coupled cavity, a metallic baffle, and the geometrical parameter symbols.

attention [34], [35]. Therefore, combining the Fano resonance with MIM plasmonic structures would create the possibility of achieving ultracompact functional optical components for use in highly integrated optics [36].

In this paper, Fano resonance is numerically investigated in a compact plasmonic system, which consists of a MIM waveguide coupled with a side cavity and a baffle. The transmission properties of the structure is analyzed by the temporal coupled mode theory (CMT) and demonstrated by the finite element method. Simulation results show that the side-coupled cavity provides a local discrete state and the baffle supports a continuous spectrum, the interaction between them, gives rise to Fano resonance. The Fano peak and dip can be easily tuned by the length of side-coupled cavity and the material embedded in the resonator. Moreover, multiple Fano resonances are achieved by extending the structure to double or more side-coupled cavities systems. This new Fano formation mechanism, based on the different states, may pave a new route to realize the Fano resonance in the plasmonic waveguide-cavity structure and may have important applications in highly integrated circuits.

2. Structure and Theoretical Analysis

The investigated waveguide system is simply composed with a MIM waveguide and a side-coupled cavity, as shown in Fig. 1. The main parameters of the structure are the length and width of the side-coupled cavity (L and w), the coupling distance (g), and the width of the bus waveguide (w). In contrast to the ordinary side-coupled system [7], a partially reflecting element (PRE) is introduced by placing a metal baffle (with thickness d) in the bus waveguide [37]. The reflection coefficient $|r_B|^2$ may be controlled by the thickness of the baffle.

In order to obtain a qualitative understanding of the optical waveguide, we analyze the transmission properties of the optical waveguide system by CMT [38]. The amplitude of the cavity is denoted by a and is normalized to the energy in the modes. The amplitudes of the incoming and outgoing waves into the cavity denoted by s_{i+} and s_{i-} $(i = 1, 2)$ (as shown in Fig. 1) and are also normalized to the power carried by the waveguide mode. The time evolution of the amplitudes of the cavity in steady state can be described as [39], [40]

$$\frac{da}{dt} = \left(-j\omega_0 - \frac{2}{\tau_a} - \frac{2}{\tau_1} - \frac{2}{\tau_2}\right)a + d_1 s_{1+} + d_2 s_{2+}. \tag{1}$$

Here, ω_0 is the resonance frequency, $1/\tau_a$ is the intrinsic cavity loss rate, $1/\tau_1$ and $1/\tau_2$ defined as the decay rates of the cavity amplitude a into the two ports, respectively, d_1 and d_2 are the input coupling coefficients associated with the forward and backward propagating modes in the bus waveguide. By power conservation, the outgoing waves are [40]

$$\begin{pmatrix} s_{1-} \\ s_{2-} \end{pmatrix} = C\begin{pmatrix} s_{1+} \\ s_{2+} \end{pmatrix} + \begin{pmatrix} d_1 \\ d_2 \end{pmatrix} a. \tag{2}$$

The scattering matrix C represents the direct coupling between incoming and outgoing waves, denoted as

$$C = \begin{pmatrix} r_B - jt_B \\ -jt_B r_B \end{pmatrix} \tag{3}$$

where r_B and t_B are the corresponding amplitude reflection and transmission coefficients, which satisfy $|r_B|^2 + |t_B|^2 = 1$, and both can be taken to be real and positive. Exploiting energy conservation and time-reversal symmetry [38], we have $d_1 = \sqrt{2/\tau_1}e^{j\theta_1}$ and $d_2 = \sqrt{2/\tau_2}e^{j\theta_2}$, herein, θ_i $(i = 1, 2)$ is the phase of coupling coefficient. Considering the symmetry of our structure, we have $\theta_1 = \theta_2$ and $\tau_1 = \tau_2 = \tau$. Therefore, the transfer function of the system can be derived as

$$t(\omega) = -jt_B - \frac{4/\tau(r_B - jt_B)}{j(\omega_0 - \omega) + 2/\tau_a + 4/\tau} \tag{4}$$

and the transmission spectrum is

$$T(\omega) = |t(\omega)|^2 = \left| t_B^2 + jt_B r_B - \frac{4/\tau}{j(\omega_0 - \omega) + 2/\tau_a + 4/\tau} \right|^2. \tag{5}$$

When the PRE is absent ($t_B = 1$, $r_B = 0$), It is obvious that the transmission spectrum exhibits a Lorentzian profile and the minimum transmission, $T_{\min} = (2/\tau_a)^2/(2/\tau_a + 4/\tau)^2$, happens when $\omega = \omega_0$, which is agree with the results in the previous papers [7], [14]. However, the presence of the PRE significantly perturbs the phase of the wave amplitudes that are directly transmitted through the waveguide, and therefore leads to complex interference phenomena, which makes the system exhibit a Fano line shape [21], [28], [37].

3. Simulations and Results

Based on the theoretical calculations presented above, the transmission properties of the waveguide system are numerically investigated using the finite element method (FEM) with COMSOL Multiphysics. Since the width of the bus waveguide is much smaller than the wavelength of the incident light, only a single propagation mode TM_0 can exist in the structure. The transmittance of SPPs is defined as the quotient between the SPP power flows of the observing port with structures (baffle and side-coupled cavity) and without structures [11], [32]. The power flows at the port were obtained by integrating the Poynting vector over the channel cross section. When a TM-polarized plane wave is injected into the MIM structure, the incident light will be coupled into the bus waveguide, and SPP waves are formed on the two metal interfaces. This system is a two-dimensional model, and the materials in the blue and white areas are chosen to be silver (ε_m), and air $(\varepsilon_d = 1.0)$, respectively. The permittivity of Ag is characterized by the Drude model: $\varepsilon_m = \varepsilon_\infty - \omega_p^2/(\omega^2 + i\omega\gamma)$ with $\varepsilon_\infty = 3.7$, $\omega_p = 9.1$ eV, $\gamma = 0.018$ eV [11], [14]. In the simulations, the parameters are set as follows: $L = 400$ nm, $w = 50$ nm, $g = 10$ nm, and $d = 20$ nm, and the values of w, g, and d are fixed throughout this paper. The calculated transmission spectra are displayed in Fig. 2(a) [no baffle] and (b) [with baffle], respectively. Fig. 2(c) and (d) show the corresponding phase response. It is obviously observed that a symmetric Lorentzian transmission line shape emerges in the transmission spectrum [see Fig. 2(a)] when the PRE is absent ($t_B = 1$, $r_B = 0$). In this case, SPPs propagates along the bus waveguide via coupling to the side-coupled cavity [7]. However, due to the presence of the PRE $(0 < r_B < 1)$, makes the coupling phase change significantly [see Fig. 2(c) and (d)], which results in a great difference in the transmission spectrum [Fig. 2(b)]. This sharp and asymmetric profile, usually termed as Fano profile [17], [18], results from the interference of the broad spectrum and the discrete resonance, which are caused by the baffle and the side-coupled cavity, respectively. These simulation results agree well with the above theoretical analysis results. The field distributions of $|H_z|^2$ for Fano resonance dip at $\lambda = 1245$ nm and peak at $\lambda = 1304$ nm, denoted by the green arrows in Fig. 2(b), are shown in Fig. 2(e) and (f), respectively. Obviously, at $\lambda = 1245$ nm, SPPs are

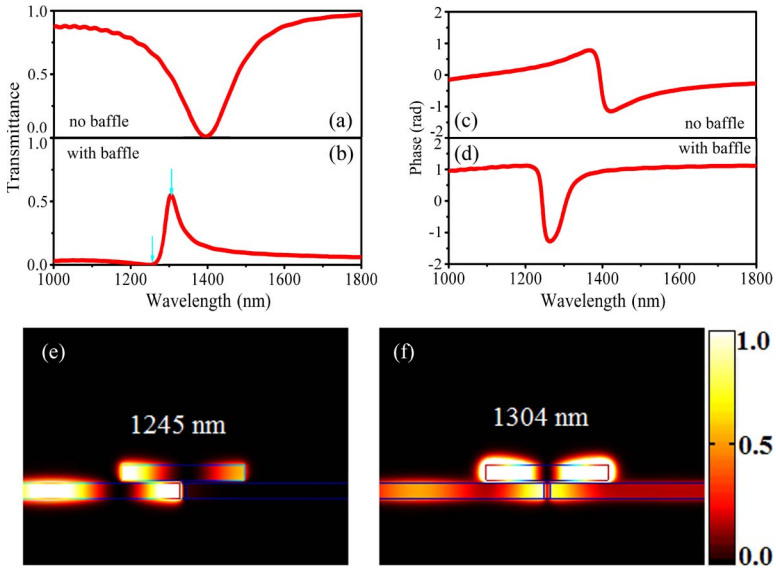

Fig. 2. (a) and (b) Transmission spectra of the optical system and (c) and (d) the corresponding phase response without and with baffle, respectively. Field distribution ($|H_z|^2$) at (e) $\lambda = 1245$ nm and (f) $\lambda = 1304$ nm.

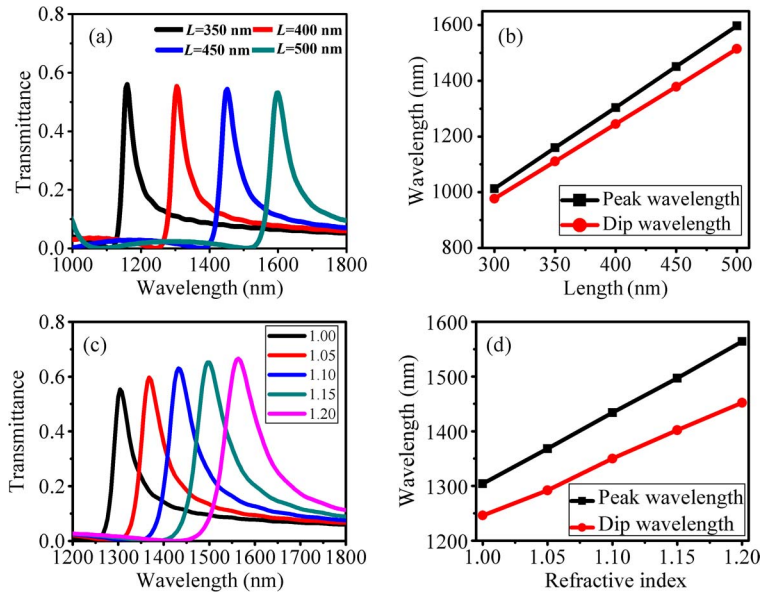

Fig. 3. (a) Transmission spectra of the optical system for different lengths of the side-coupled cavity. (b) Dependence of the resonant wavelengths on length *L*. (c) Transmission spectra of the optical system for different refractive index in the side-coupled cavity. (d) Transmitted-peak wavelength of Fano resonance versus refractive index.

almost blocked at the PRE, acted as the "off" state, while at $\lambda = 1304$ nm, SPPs can pass through the waveguide to the output port, served as the "on" state. In the all optical communication system, Fano profile is generally used to realize all-optical plasmonic switches [20], [26]. In our structure, the Fano on/off contrast ratio can be achieved to 30 dB by adding the PRE, while it is only 20 dB for the Lorentzian profile.

Next, we investigated the transmission properties of the proposed structure using FEM. Fig. 3(a) shows the calculated transmission spectra for different length of the side-coupled cavity. Fig. 3(b)

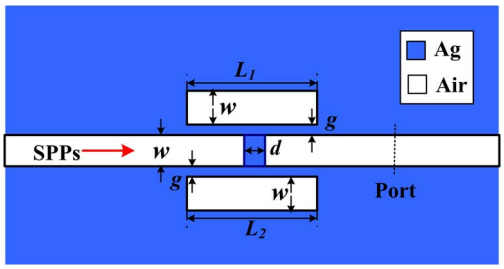

Fig. 4. Schematic of the optical system consisting of an MIM waveguide with a two side-coupled cavity in each side, a metallic baffle, and the geometrical parameter symbols.

displays the dependence of the resonant wavelengths on length L. It is obvious that both the Fano resonant dip and peak are proportional to the length L. Specially, we can find that the difference between the resonant peak and dip increases with the length increasing, which may attribute to the internal loss increases when the length increases. According to the simulation results, the Fano resonance wavelengths can be easily manipulated by adjusting the length of the side-coupled cavity.

Successively, we investigate the influence of the material embedded in the side-coupled cavity on the Fano resonance wavelength. The length of the side-coupled cavity is set to be 400 nm. By changing the refractive index, the center wavelength exhibits a red-shift as shown in Fig. 3(c). As can be seen from Fig. 3(d), it is found that the transmitted-peak and -dip wavelength both have a nearly linear relationship with the refractive index. Therefore, one can simply manipulate the Fano resonance wavelength by fitting the material with appropriate refractive index in the side-coupled cavity. Besides, the proposed structure can be served as a high sensitivity nanosensor with the sensitivity of 1280 nm/RIU (per unit variations of the refractive index) [11], [12]. However, some challenges that we may be faced if the device was actually made to the practical applications, for example, it is difficult to fabricate such a thin free-standing structure $(\mathrm{g} = 10\ \mathrm{nm})$, and the infiltrated fluids may damage the thin Ag spacers in the context of the current technology. Anyhow, the proposed structure achieved a sharp and asymmetric Fano profile, which has a wide application in nano-devices.

4. Multiple Fano Resonances Induced by Adding Another Side-Coupled Cavity

4.1 Adding a Side-Coupled Cavity in the Opposite Side

According to the above characteristics of the plasmonic system based on side-coupled cavity, the proposed Fano structure in Fig. 1 is flexible and can be easily extended to a multiple Fano resonances system by adding another side-coupled cavity, as shown in Fig. 4. Based on the theoretical analysis in Section 2, we know that the SPPs propagate along the bus waveguide, one portion of them coupled to the upper cavity, the other to the lower cavity, both of them will interference with the third portion, which pass through the baffle, resulting in Fano resonances. By carefully adjusting the parameters of the structure, we can separate the two Fano resonances. To display the phenomenon intuitively, the transmission spectra of the proposed structure are simulated with FEM, and the calculated transmission spectra are shown in Figs. 5(a)–(e). It is obviously observed that two Fano profiles emerge in the transmission spectra. Moreover, one of them exhibits a red shift [denoted by the green arrows] with L_2 increases, the other keeps unchanged due to L_1 is fixed to 400 nm. That is to say, the green-arrow denoted Fano peaks are determined by the lower cavity, while the others are determined by the upper cavity. Figs. 5(f)–(j) shows the corresponding field distributions of $|H_z|^2$ at the green-arrow positions for different length L_2. It is observed that the energy almost distributes in the lower cavity, except for Fig. 3(c). These behaviors of the two Fano resonances accord well with the analysis.

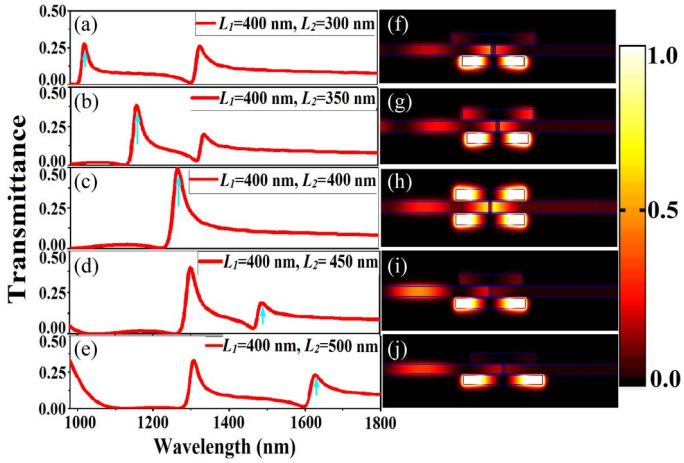

Fig. 5. Simulation results of the transmission spectra at $L_1 = 400$ nm. (a) $L_2 = 300$ nm, (b) $L_2 = 350$ nm, (c) $L_2 = 400$ nm, (d) $L_2 = 450$ nm, and (e) $L_2 = 500$ nm. Corresponding field distributions ($|H_z|^2$) of the system at the green-arrow positions for different lengths L_2 of (f–j).

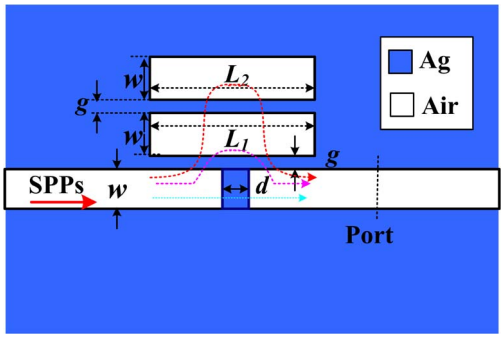

Fig. 6. Schematic of the optical system consisting of an MIM waveguide with two side-coupled cavity in one side, a metallic baffle, and the geometrical parameter symbols.

4.2 Adding a Side-Coupled Cavity up the Original One

In this part, we analyze the case that waveguide coupling for the two side-coupled cavity in one side, which is shown in Fig. 6. The propagation behaviors of SPPs can be illustrated by the three dotted lines, and these SPPs with different paths will be interference with each other at the output port, which may enrich the transmission spectra. The two side cavities are directly coupling with each other by a coupling coefficient μ. The resonant frequencies for a and b are ω_a and ω_b, while the intrinsic loss are $1/\tau_a$ and $1/\tau_b$, respectively, and the other parameters are the same with that in Fig. 1. For Fig. 6, the CMT equations are given [39]

$$\frac{da}{dt} = \left(-j\omega_a - \frac{2}{\tau_a} - \frac{2}{\tau_1} - \frac{2}{\tau_2}\right)a + d_1 s_{1+} + d_2 s_{2+} - j\mu b \tag{6}$$

$$\frac{db}{dt} = \left(-j\omega_b - \frac{2}{\tau_b}\right)b - j\mu a. \tag{7}$$

Following the same procedure, we can obtain the transfer functions as follows:

$$t(\omega) = -jt_B - \frac{2[j(\omega_b - \omega) + 2/\tau_b](r_B - jt_B)/\tau}{[j(\omega_a - \omega) + 2/\tau_a + 4/\tau][j(\omega_b - \omega) + 2/\tau_b] + \mu^2}. \tag{8}$$

Equation (8) indicates that this system can support multiple Fano resonances. To better demonstrate the phenomena, the transmission spectra are calculated, which are shown in

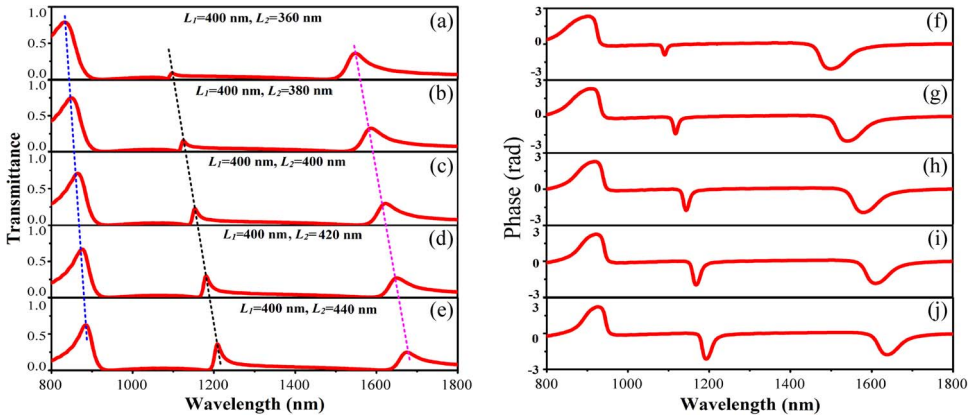

Fig. 7. Simulation results of the transmission spectra at $L_1 = 400$ nm. (a) $L_2 = 360$ nm, (b) $L_2 = 380$ nm, (c) $L_2 = 400$ nm, (d) $L_2 = 420$ nm, and (e) $L_2 = 440$ nm. Corresponding phase response of the system for different lengths $L2$ of (f–j).

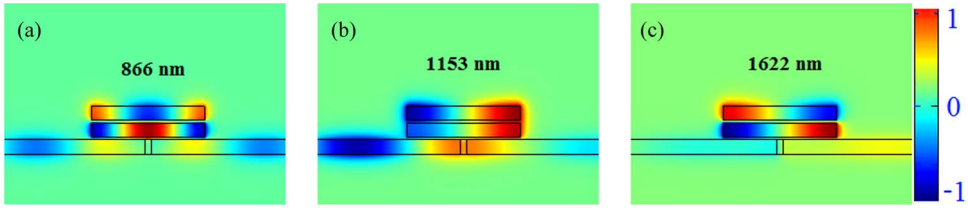

Fig. 8. Corresponding field distributions (Hz) of the Fig. 6 at $L_1 = 400$ nm and $L_2 = 400$ nm for (a) $\lambda = 866$ nm, (b) $\lambda = 1153$ nm, and (c) $\lambda = 1622$ nm.

Figs. 7(a)–(e), and the corresponding phase response are also plotted in Figs. 7(f)–(j), respectively. Herein, the parameters are set with a fixed $L_1 = 400$ nm, and an alterable L_2. It is found that three Fano peaks appear in the transmission spectra, and all of them are red-shift linearly [denoted by the dotted lines] with increasing L_2. In order to understand the underlying physics of the resonant peaks in the transmission spectra, the field distributions of H_z at the Fano peaks, with $L_1 = 400$ nm and $L_2 = 400$ nm, are displayed in Figs. 8(a)–(c). Obviously, the first Fano resonance [indicated by the blue dotted line in Fig. 7] is caused by the higher order mode excited, the other two Fano resonances [one is high energy, denoted by the black dotted line, the other is low energy, denoted by the pink dotted line] are aroused by the lower resonant mode, and they are degenerate. The difference between the two Fano peaks is that the phase of H_z in the adjacent of the two side-coupled cavities are inphase and antiphase for the high energy and low energy Fano peak, respectively. According to the above results, the multiple Fano resonances are induced by the phase coupled effects [10].

According to the above analysis, the structure of Fig. 6 can be easily extend to a four resonator-coupled system [inset in Fig. 9]. Fig. 9 shows the transmission spectrum of the system. Herein, the four side-coupled cavity are set, for simplicity, the same with $L = 400$ nm. It is obvious that six Fano resonance peaks occur in the transmission spectrum, which are caused by the complex interference with multiple paths of SPPs. The multi-resonator-coupled system with multi-Fano profiles' optical responses may have complex functional applications, such as sensors, splitter multichannel switches, and wavelength-division multiplexing.

5. Summary

In summary, the transmission characteristics of the proposed structure, which consists of a MIM waveguide with a side-coupled cavity and a baffle, are analyzed and investigated. Simulation results show that by introducing a metal baffle, which supports a continuous state, the phase of

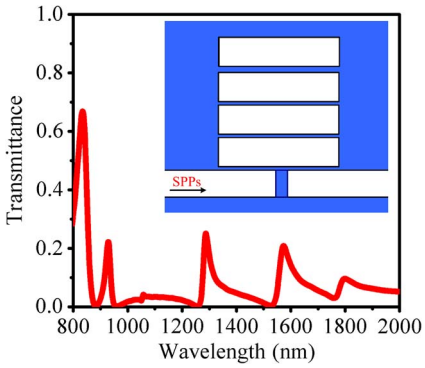

Fig. 9. Transmission spectrum of the four resonator-coupled system. (Inset) Schematic of the four-resonator-coupled system.

the wave amplitudes that are directly transmitted through the waveguide is significantly perturbed, and then a sharp and asymmetric Fano profile emerges in the transmission spectrum. The Fano line shape can be easily tuned by changing the parameters of the structure. In addition, multiple Fano resonances are achieved by extending the structure to several types. The utilization of a baffle creates a new path for realizing Fano resonance in the plasmonic waveguide-cavity system.

References

[1] W. L. Barnes, A. Dereux, and T. W. Ebbesen, "Surface plasmon subwavelength optics," *Nature*, vol. 424, no. 6950, pp. 824–830, Aug. 2003.
[2] T. Xu, Y. K. Wu, X. G. Luo, and L. J. Guo, "Plasmonic nanoresonators for high-resolution colour filtering and spectral imaging," *Nat. Commun.*, vol. 1, p. 59, Aug. 2010.
[3] G. Veronis and S. H. Fan, "Bends and splitters in metal-dielectric-metal subwavelength plasmonic waveguides," *Appl. Phys. Lett.*, vol. 87, Sep. 2005, Art. ID. 131102.
[4] E. N. Economou, "Surface plasmons in thin films," *Phys. Rev.*, vol. 182, no. 2, p. 539, Jun. 1969.
[5] X. S. Lin and X. G. Huang, "Tooth-shaped plasmonic waveguide filters with nanometeric sizes," *Opt. Lett.*, vol. 33, no. 23, pp. 2874–2876, Dec. 2008.
[6] A. Hosseini and Y. Massoud, "Nanoscale surface plasmon based resonator using rectangular geometry," *Appl. Phys. Lett.*, vol. 90, no. 18, Apr. 2007, Art ID. 181102.
[7] Q. Zhang, X. G. Huang, X. S. Lin, J. Tao, and X. P. Jin, "A subwavelength coupler-type MIM optical filter," *Opt. Exp.*, vol. 17, no. 9, pp. 7549–7554, Apr. 2009.
[8] J. Tao, X. G. Huang, X. S. Lin, Q. Zhang, and X. P. Jin, "A narrow-band subwavelength plasmonic waveguide filter with asymmetrical multiple teeth-shaped structure," *Opt. Exp.*, vol. 17, no. 16, pp. 13 989–13 994, Jul. 2009.
[9] J. J. Chen *et al.*, "Plasmonic Y-splitters of high wavelength resolution based on strongly coupled-resonator effects," *Plasmonics*, vol. 7, no. 3, pp. 441–445, Jan. 2012.
[10] Z. Chen *et al.*, "Spectral splitting based on electromagnetically induced transparency in plasmonic waveguide resonator system," *Plasmonics*, vol. 10, no. 3, pp. 721–727, Dec. 2014.
[11] Z. Chen and L. Yu, "Multiple fano resonances based on different waveguide modes in a symmetry breaking plasmonic system," *IEEE Photon. J.*, vol. 6, no. 6, Nov. 2014, Art ID. 4802208.
[12] H. Lu, X. M. Liu, D. Mao and G. X. Wang, "Plasmonic nanosensor based on Fano resonance in waveguide-coupled resonators," *Opt. Lett.*, vol. 37, no. 18, pp. 3780–3782, Sep. 2012.
[13] Z. P. Zhou, F. F. Hu, and H. X. Yi, "Wavelength demultiplexing structure based on arrayed plasmonic slot cavities," *Opt. Lett.*, vol. 36, no. 8, pp. 1500–1502, Apr. 2011.
[14] G. X. Wang, H. Lu, X. M. Liu, D. Mao, and L. N. Duan, "Tunable multi-channel wavelength demultiplexer based on MIM plasmonic nanodisk resonators at telecommunication regime," *Opt. Exp.*, vol. 19, no. 4, pp. 3513–3518, Feb. 2011.
[15] A. Noual, A. Akjouj, Y. Pennec, J. Gillet, and B. Djafari-Rouhani, "Modeling of two-dimensional nanoscale Y-bent plasmonic waveguides with cavities for demultiplexing of the telecommunication wavelengths," *New J. Phys.*, vol. 11, no. 10, Oct. 2009, Art ID. 103020.
[16] H. Lu, X. M. Liu, Y. K. Gong, D. Mao, and L. R. Wang, "Enhancement of transmission efficiency of nanoplasmonic wavelength demultiplexer based on channel drop filters and reflection nanocavities," *Opt. Exp.*, vol. 19, no. 14, pp. 12 885–12 890, Jun. 2011.
[17] U. Fano, "Effects of configuration interaction on intensities and phase shifts," *Phys. Rev.*, vol. 124, no. 6, pp. 1866–1878, Dec. 1961.

[18] A. Miroshnichenko, S. Flach, and Y. Kivshar, "Fano resonances in nanoscale structures," *Rev. Mod. Phys*., vol. 82, no. 3, pp. 2257–2298, Aug. 2010.
[19] B. Luk'yanchuk *et al*., "The Fano resonance in plasmonic nanostructures and metamaterials," *Nat. Mater*., vol. 9, no. 9, pp. 707–715, Sep. 2010.
[20] J. J. Chen, Z. Li, X. Zhang, J. H. Xiao, and Q. H. Gong, "Submicron bidirectional all-optical plasmonic switches," *Sci. Rep*., vol. 3, p. 1451, Mar. 2013.
[21] M. Heuck, P. T. Kristensen, Y. Elesin, and J. Mork, "Improved switching using Fano resonances in photonic crystal structures," *Opt. Lett*., vol. 38, no. 14, pp. 2466–2468, Jul. 2013.
[22] J. J. Chen, Z. Li, J. Li, and Q. H. Gong, "Compact and high-resolution plasmonic wavelength demultiplexers based on Fano interference," *Opt. Exp*., vol. 19, no. 10, pp. 9976–9985, May 2011.
[23] Z. Chen *et al*., "Plasmonic wavelength demultiplexers based on tunable Fano resonance in coupled-resonator systems," *Opt. Commun*., vol. 320, pp. 6–11, Jan. 2014.
[24] A. Cetin and H. Altug, "Fano resonant ring/disk plasmonic nanocavities on conducting substrates for advanced biosensing," *ACS Nano*, vol. 6, no. 11, pp. 9989–9995, Oct. 2012.
[25] Y. H. Fu, J. B. Zhang, Y. F. Yu, and B. Luk'yanchuk, "Generating and manipulating higher order Fano resonances in dual-disk ring plasmonic nanostructures," *ACS Nano*, vol. 6, no. 6, pp. 5130–5137, Jun. 2012.
[26] K. Nozaki *et al*., "Ultralow-energy and high-contrast all-optical switch involving Fano resonance based on coupled photonic crystal nanocavities," *Opt. Exp*., vol. 21, no. 10, pp. 11 877–11 888, May 2013.
[27] Y. Yu *et al*., "Fano resonance control in a photonic crystal structure and its application to ultrafast switching," *Appl. Phys. Lett*., vol. 105, no. 6, Aug. 2014, Art. ID. 061117.
[28] Y. Yu *et al*., "Nonreciprocal transmission in a nonlinear photonic-crystal Fano structure with broken symmetry," *Laser Photon. Rev*., vol. 9, no. 2, pp. 241–247, Jan. 2015.
[29] L. V. Brown, H. Sobhani, J. B. Lassiter, P. Nordlander, and N. J. Halas, "Heterodimers: Plasmonic properties of mismatched nanoparticle pairs," *ACS Nano*, vol. 4, no. 2, pp. 819–832, Feb. 2010.
[30] M. Rahmani, B. Luk'yanchuk, and M. H. Hong, "Fano resonance in novel plasmonic nanostructures," *Laser Photon. Rev*., vol. 7, no. 3, pp. 329–349, Jun. 2012.
[31] J. Wang *et al*., "Double Fano resonances due to interplay of electric and magnetic plasmon modes in planar plasmonic structure with high sensing sensitivity," *Opt. Exp*., vol. 21, no. 2, pp. 2236–2244, Jan. 2013.
[32] Z. Chen, J. J. Chen, L. Yu, and J. H. Xiao, "Sharp trapped resonances by exciting the anti-symmetric waveguide mode in a metal-insulator-metal resonator," *Plasmonics*, vol. 10, no. 1, pp. 131–137, Sep. 2014.
[33] X. J. Piao, S. Yu, S. Koo, K. Lee, and N. Park, "Fano-type spectral asymmetry and its control for plasmonic metal-insulator-metal stub structures," *Opt. Exp*., vol. 19, no. 11, pp. 10907–10912, May 2011.
[34] V. A. Fedotov, M. Rose, S. L. Prosvirnin, N. Papasimakis, and N. I. Zheludev, "Sharp trapped-mode resonances in planar metamaterials with a broken structural symmetry," *Phys. Rev. Lett*., vol. 99, no. 14, Apr. 2007, Art ID. 147401.
[35] J. W. Qi *et al*., "Independently tunable double Fano resonances in asymmetric MIM waveguide structure," *Opt. Exp*., vol. 22, no. 12, pp. 14 688–14 695, Jun. 2014.
[36] N. Liu *et al*., "Plasmonic analogue of electromagnetically induced transparency at the drude damping limit," *Nat. Mater*., vol. 8, pp. 758–762, Sep. 2009.
[37] S. H. Fan, "Sharp asymmetric line shapes in side-coupled waveguide-cavity systems," *Appl. Phys. Lett*., vol. 80, no. 6, pp. 908–910, Aug. 2002.
[38] H. A. Haus, *Waves and Fields in Optoelectronics*. New York, NY, USA: Prentice-Hall, 1984.
[39] Q. Li, T. Wang, Y. Su, M. Yan, and M. Qiu, "Coupled mode theory analysis of mode-splitting in coupled cavity system," *Opt. Exp*., vol. 18, no. 8, pp. 8367–8382, Apr. 2010.
[40] W. Soo, Z. Wang, and S. H. Fan, "Temporal coupled-mode theory and the presence of non-orthogonal modes in lossless multimode cavities," *IEEE J. Quantum. Electron*., vol. 40, no. 10, pp. 1511–1518, Oct. 2004.